FOURIER-TRANSFORM IMAGING FOR X-RAY ASTRONOMY

G. J. Hurford and H. S. Hudson*

California Institute of Technology
Solar Astronomy 264-33
Pasadena, California 91125

March 1980
BBSO #0188
(UCSD-SP-79-27)

*University of California, San Diego, La Jolla, CA 92093, U.S.A.

ABSTRACT

A Fourier-transform telescope for X-ray astronomy can be constructed from several modulation collimators [1,10]. We show in detail how this permits a precise mathematical analogy with the theory of aperture synthesis in radio astronomy, with each individual modulation collimator or "subcollimator" providing the measurement of a single Fourier component of the source angular distribution. Constructing a Fourier-transform telescope with one-dimensional imaging collimators obviates the need for mechanical scanning, so that time-variable sources such as solar flares can be accurately mapped without space/time confusion. Other advantages of a Fourier-transform approach for X-ray imaging include (i) high aperture efficiency, (ii) the multiplex advantage across a chosen field of view, (iii) relatively simple structural and thermal requirements as compared with a multiple-grid collimator, (iv) a need for only a modest position sensitivity in the detector, and (v) high angular resolution with a relatively compact telescope.

1. Introduction

Conventional imaging techniques use reflection or refraction of the incident radiation. Since these processes do not work well at wavelengths $\lesssim 2\text{Å}$ image formation must rely on non-focusing collimation techniques. The simplest form of collimator - the slat collimator, "lead pipe telescope", or Soller collimator - has found wide application in X-ray astronomy because it maximizes the signal from a known source while at the same time reducing the background counting rate from unwanted sources. This approach works most efficiently for a source whose location and angular size are already known.

The (two-grid) modulation collimator introduced by Oda [1] represented the first advance in collimator sophistication in X-ray astronomy. We illustrate its principles in Figure 1. The modulation collimator has the advantage of simultaneous measurements of signal and background; it also has the ability to locate a source whose existence or location is not previously known. Extending the concept to multiple grids [2] or rotational scanning [3] permits the formation of true images, either continuously spread across the image plane [2] or subdivided into discrete picture elements by subcollimators that feed independent counter elements [4]. A practical limit on the angular resolution of these multiple-grid collimators is the need for mechanical rigidity of the support structure. The structure must maintain the relative positions of the grids to a fraction of the individual hole size, which in practical systems [4] may be as small as 50μ. In principle the formation of images with a single grid [5,6,7] avoids the need for a precise structure. The effective area of one of these

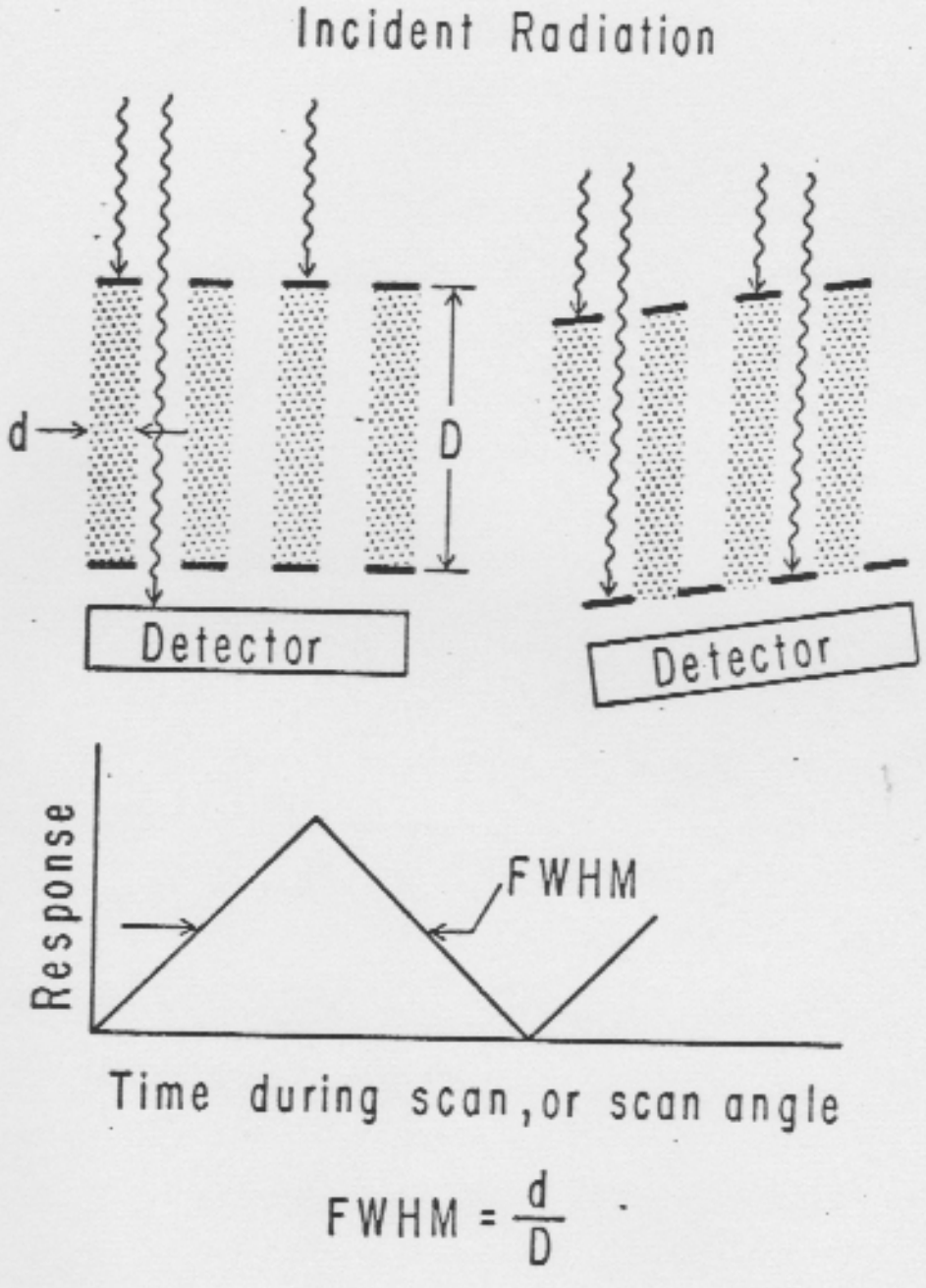

$$FWHM = \frac{d}{D}$$

Figure 1. Principles of operation of the two-grid modulation collimator, showing how a point source produces a triangle-wave modulation of the counting rate as the collimator sweeps in angle. The angular resolution is determined by the ratio of hole size to collimator length.

multiple pinhole arrays may be quite large, and recent developments [8,9] have shown that they may have an image quality as good as that of a simple pinhole camera. In terms of high angular resolution, the position sensitivity of the detector provides a practical limit.

A recent suggestion for a two-grid collimator [10] may combine high resolution with moderate structural stability requirements. Makishima et al. [10] refer to this concept as the multi-pitch modulation collimator (MPMC); it consists of a set of two-grid modulation collimators each with a different aperture spacing and/or orientation. Given an aperture spacing, sources smaller than the corresponding angular scale will give modulated signals as the collimator scans the sky, as shown in Figure 1. The key concept of the MPMC consists of the fact that the fundamental Fourier component of the signal modulation measures the corresponding Fourier component of the angular distribution of the source. Thus a single subcollimator determines the identical parameter measured by a two-element interferometer as used in radio astronomy. As in aperture synthesis [11], a number of such measurements can be combined to produce an image.

In sections that follow, we formally establish the analogy to radio astronomy (Section 2) and show how to make the Fourier component measurements instantaneously, without mechanically scanning (Section 3). Section 4 discusses the practical limits of these ideas, and Section 5 discusses the performance of X-ray imaging systems on a comparative basis.

2. ANALOGY WITH RADIO ASTRONOMY

The response of a two-element interferometer in radio astronomy may be written as

$$R(t) = \mathrm{Re}\left\{ e^{2\pi i \vec{B}\cdot\vec{S}(t)} \int_{-\infty}^{\infty} d\vec{\sigma}\; I(\vec{\sigma})\; e^{2\pi i \vec{b}(t)\cdot\vec{\sigma}} \right\} \qquad (1)$$

where $\vec{B}$ is the physical baseline (in units of wavelength), $\vec{b}(t)$ is its projection orthogonal to the source direction, $\vec{S}(t)$, and $I(\vec{\sigma})$ is the source brightness distribution as seen by the primary beam of each antenna (Fomalont and Wright [11], equation 10.11). Since the time variability is normally due to the diurnal source motion, the instantaneous response can be rewritten as

$$R = \mathrm{Re}\left\{ K \int_{-\infty}^{\infty}\int_{-\infty}^{\infty} dx\, dy\; I(x,y)\; e^{2\pi i(ux + vy)} \right\} \qquad (2)$$

where K is independent of the source and the integral has been explicitly written in terms of eastward and northward displacements (x,y) on the sky, and (u,v) are the corresponding components of $\vec{b}(t)$. Note that the response depends only on the spatial-frequency content in the source that corresponds to u and v.

Equation 2 can be further simplified by rewriting the integral in terms of (θ,ϕ), orthogonal coordinates in the sky parallel and perpendicular to $\vec{b}$,

$$R = \mathrm{Re}\left\{ K \int_{-\infty}^{\infty} d\theta\; F(\theta)\; e^{2\pi i\, b\theta} \right\} \qquad (3)$$

where $F(\theta) = \int_{-\infty}^{\infty} d\phi\; I(\theta,\phi)\; d\phi$ is the projection of the source brightness distribution perpendicular to $\vec{b}$.

For a given source location, the baseline orientation determines the orientation of the coordinates (θ,ϕ), the fringe orientations, and the baseline length (in units of wavelength) determines $|\vec{b}|$ (= 1/fringe spacing).

To characterize the response of the modulation collimator in X-ray astronomy, we represent the transmission pattern (Fig. 1) by a triangle wave $\Lambda(\theta)$ that repeats with angular period P:

$$\Lambda(\theta) = 1 - 2|\theta|/P \quad -P/2 \leq \theta \leq P/2$$
$$\Lambda(\theta \pm P) = \Lambda(\theta). \tag{4}$$

A scanning modulation collimator will sweep out the angular range P during a finite time, and the counting rate as a function of time must be converted to the angular profile from an aspect solution that describes the collimator motion. We can make a more complete model of the angular response with a function $N(\theta)$ such that $N(\theta)\Delta\theta$ is the probability of ΔN counts in the angular range $\Delta\theta$:

$$N(\theta) = A \int_{-\infty}^{\infty} [0.5\, F(\psi)\, \Lambda(\theta - \psi) + B]\, \Delta t\, d\psi \tag{5}$$

where $F(\psi)$ is the source brightness contribution $[\text{ph}(\text{cm}^2\ \text{sec radian})^{-1}]$ integrated parallel to the collimator aperture (we have assumed a 50% maximum response); B is the background rate in counts $(\text{cm}^2\ \text{sec})^{-1}$, A the detector area (cm^2) and Δt the integration time (sec).

To establish the precise analogy with Equation (1), we define

$$V = \frac{2}{P} \int_{-P/2}^{P/2} N(\theta)\, e^{i\frac{2\pi}{P}\theta}\, d\theta \tag{6}$$

to be the complex visibility function measured by the given collimator. In practice this will represent a sum over time-binned data. Substituting (5) in (6), we obtain

$$V = \frac{A}{P}\int_{-\infty}^{\infty}\int_{-P/2}^{P/2}[F(\psi)\ \Lambda(\Theta-\psi) + 2B]\ \Delta t\ e^{i\frac{2\pi}{P}\Theta}\ d\Theta\ d\psi \qquad (7)$$

Since $\Lambda(\Theta-\psi)$ is periodic, this becomes

$$V = \frac{A}{P}\int_{-\infty}^{\infty}\int_{-P/2}^{P/2}F(\psi)\ \Lambda(\Theta)\ \Delta t\ e^{i\frac{2\pi}{P}(\Theta+\psi)}\ d\Theta\ d\psi \qquad (8)$$

and substituting for $\Lambda(\Theta)$ gives

$$V = \int_{-\infty}^{\infty}\frac{2\ AF(\psi)\ \Delta t}{\pi^2}\ e^{i\frac{2\pi}{P}\psi}\ d\psi \qquad (9)$$

whence

$$\mathrm{Re}(V) = \mathrm{Re}\left\{\mathrm{const}\int_{-\infty}^{\infty}F(\psi)\ e^{\frac{2\pi i\psi}{P}}\ d\psi\right\} \qquad (10)$$

in the same form as Equation (3), establishing the precise analogy. This opens up for X-ray astronomy the use of all of the nomenclature and methods of analysis of radio astronomy. Note that this identity really is fortuitous, since for radio waves the characteristic sinusoidal variation of response with angle comes from wave interference, while for X-rays it comes from geometrical shadowing.

A Fourier-transform telescope consists of a set of individual modulation collimators (subcollimators) that feed discrete detector

units. A subcollimator is equivalent to one baseline or a simple two-element interferometer in radio astronomy. A measurement of the amplitude $V = [Re(V)]^2 + [Im(V)]^2$ and phase $\psi = \tan^{-1}[Im(V)/Re(V)]$ determines all of the necessary information regarding the Fourier component measured by a given subcollimator. Imaging results from the inverse Fourier transformation of the visibility $V(u,v)$, considered as a function of the angular wavenumbers (u,v) defined by the collimator period $P = 1/\sqrt{u^2 + v^2}$ and orientation. A complete and well-defined image requires the measurement of $V(u,v)$ at a sufficiently dense [12] set of points in the (u,v)-plane. Standard texts on radio astronomy [13,14] give full details of these manipulations.

3. INSTANTANEOUS MEASUREMENT OF THE VISIBILITY

The scanning modulation collimator has the well-known property of sensitivity to time variations, either in the source flux or in the background. Time variability in background or source flux can mimic the spatial modulations, thus causing uncertainty in their interpretation. Hard X-ray observations are generally background-limited and also frequently subject to such variabilities, and so the problem of space-time confusion is an important one.

The imaging modulation collimator [2] (Figure 2) makes it possible to measure a visibility function without scanning. As illustrated in Figure 2, a two-grid collimator can project a one-dimensional image of an X-ray source onto a detector such as a position-sensitive proportional counter. The dispersion of the image can be chosen arbitrarily by the selection of the grid geometry. In the simplest configuration, n + 1

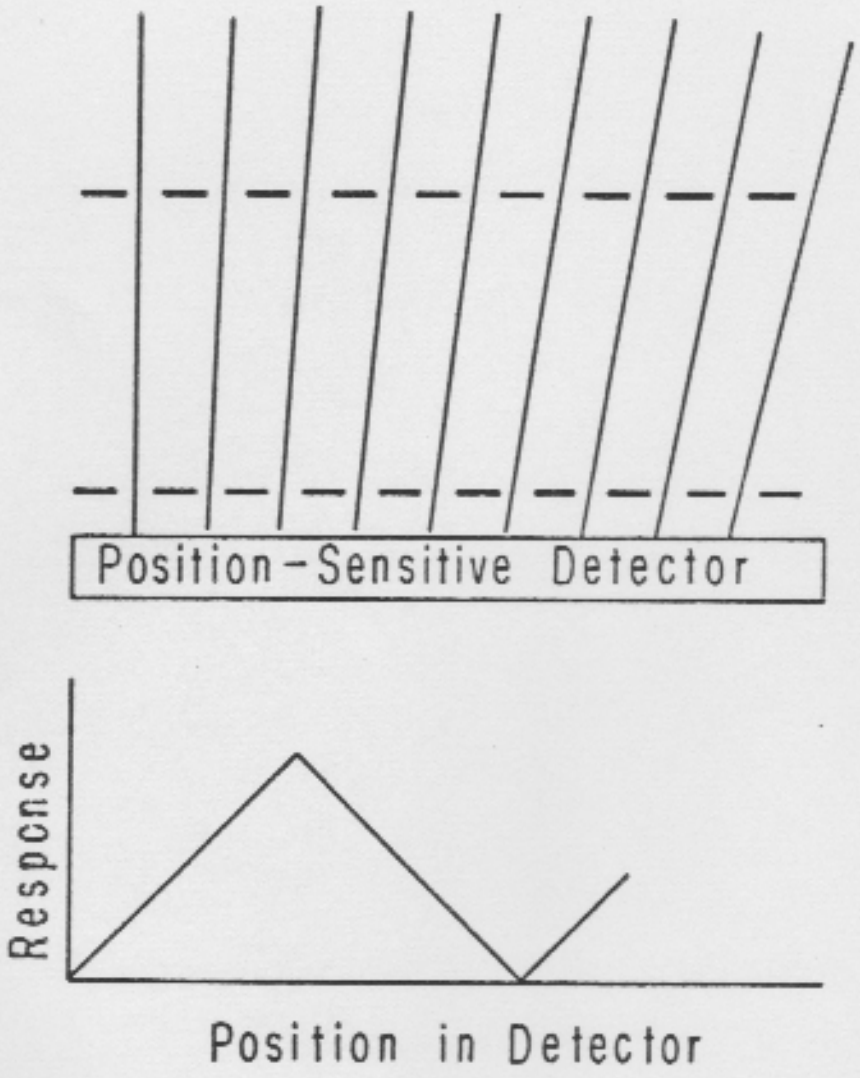

Figure 2. Principle of operation of a simple imaging modulation collimator. The lower grid has slightly smaller holes than the upper grid. The response as a function of position in the detector has the same triangle-wave nature as the time function in Figure 1. The angular resolution is the same (FWHM = d/D) but the position dispersion of the "image" may be varied by changing the grid parameters slightly.

apertures in the front grid and n apertures in the back grid distribute exactly one period of a triangular response pattern across the detector area. This spatial triangular response is equivalent to the temporal triangular response illustrated in Figure 1. A point source at any angle ψ will produce a peak counting rate somewhere on the detector; the location of this peak corresponds to ψ and its amplitude determines $|V|$. Thus a simple two-grid imaging collimator with a position-sensitive detector can measure one Fourier component of the source angular distribution.

The combination of data from many such subcollimators, each with its position-sensitive readout, permits the synthesis of an image as discussed above. The illustration in Figure 3 suggests an obvious means of constructing an imaging system, with the subcollimators distributing the modulated count-rate along the sensitive dimension of a position-sensitive detector. Different slit orientations and spacings generate the different Fourier components needed. In essence the Fourier-component measurement consists of a three-parameter fit ($|V|$, ψ, s) to each subcollimator output, where s is the mean count level. This dictates a position sensitivity sufficient to accomplish the measurement, as described in Section 4 in detail; in practice a useful hard X-ray telescope must have a large area and the requirements for position sensitivity are therefore not severe. The form of the count-rate distribution is similar for each subcollimator, independent of the slit spacing and the orientation of the grids. Figure 4 illustrates this, with different ($|V|$, ψ) combinations for several subcollimators. We note

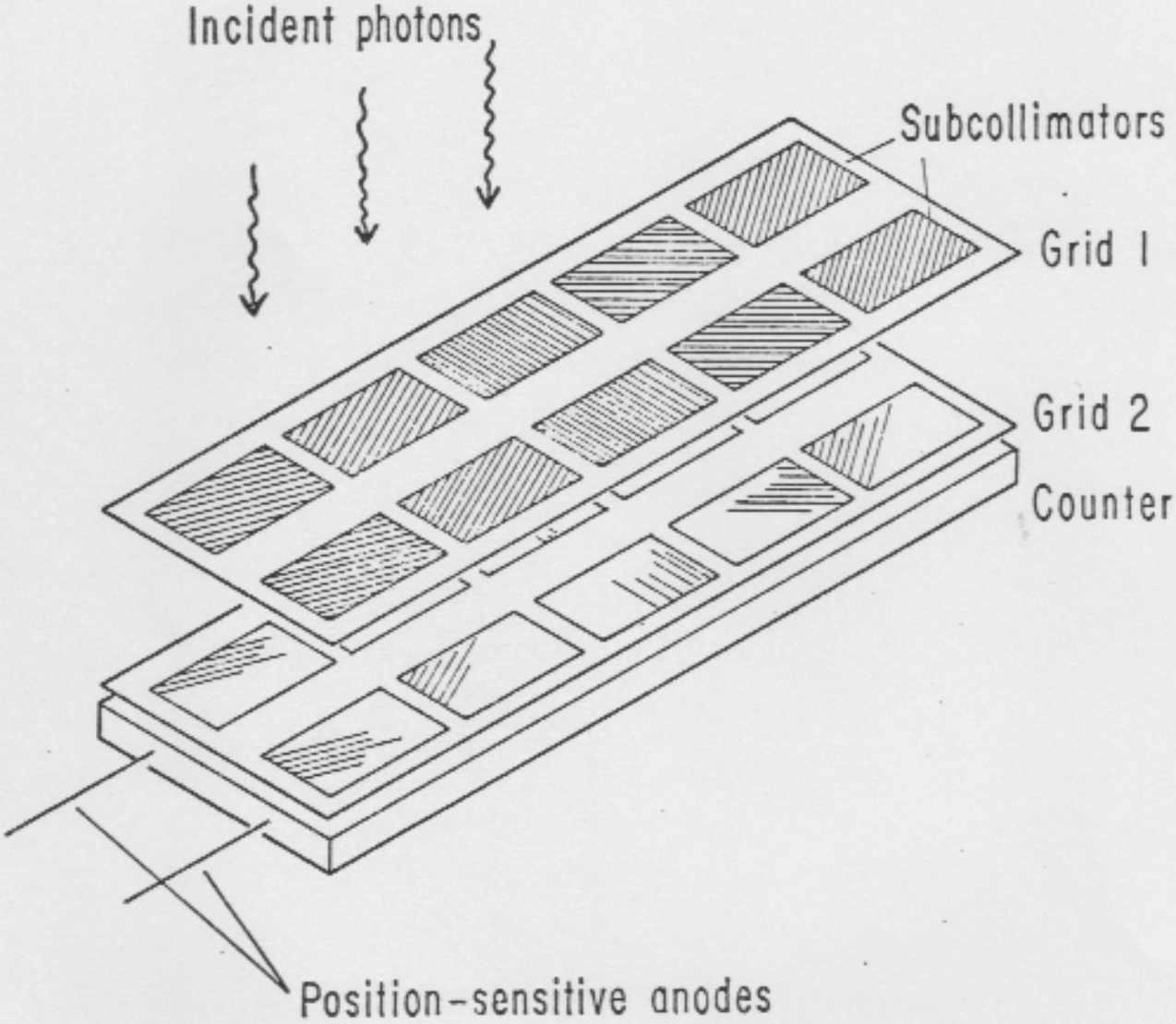

Figure 3. Sketch of layout for a two-grid imaging collimator and a position-sensitive proportional counter. The wire spacings differ (as illustrated in Figure 2) so that one Fourier component is distributed along the direction of position sensitivity. The slits do not need to have the same orientation as this direction: the sketch shows ten individual subcollimators or "baselines".

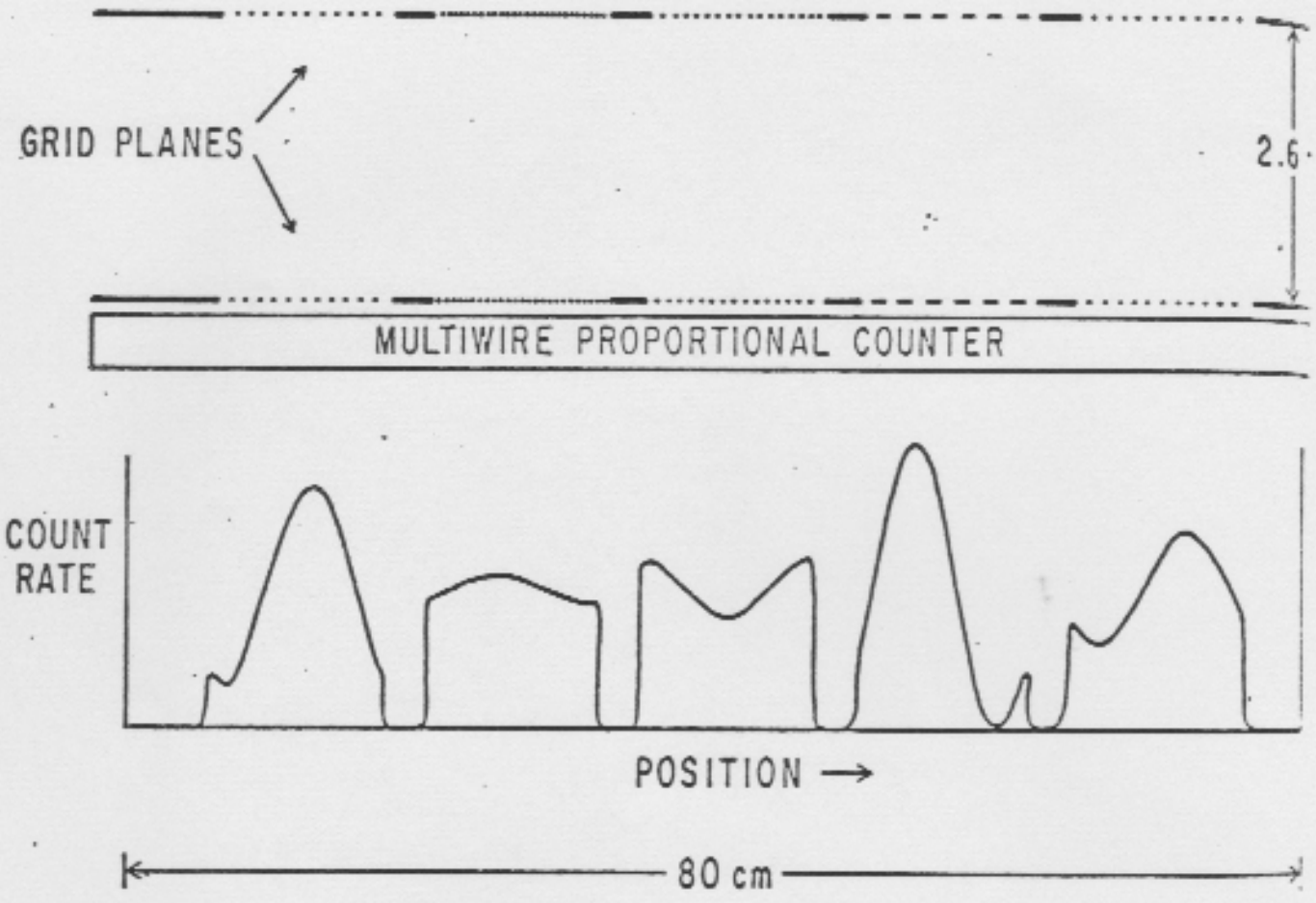

Figure 4. Schematically illustrates the count distribution in five subcollimators (see Fig. 3) with position-sensitive proportional-counter readout. Each subcollimator has different angular parameters and a different visibility.

that if the subcollimators have the same field of view and the detector properties are identical, the mean counting rate(s) should be the same for each. This gives an additional check on telescope performance.

4. PRACTICAL LIMITATIONS

We describe in this section some of the constraints imposed by practical considerations in the construction of Fourier-transform telescopes for X-ray astronomy. The configuration is assumed to be that sketched in Figures 3 and 4, namely an array of one-dimensional imaging subcollimators with position-sensitive readout.

(a) Coverage in the (u,v)-plane.

The optimum selection of coverage in the (u,v)-plane will not be discussed in detail in this paper; in general the experience of radio astronomy can again serve as a guide. One should aim at complete coverage if true imaging is an important goal, for example with spatially complex sources or if confusion of numerous point-source images is a problem. If simple models of a few sources can adequately represent the image, then limited (u,v)-plane coverage may be appropriate. In general, dividing a given counter area into a larger number of subcollimators does not drastically reduce the point-source effective area, although it does affect the precision with which each visibility can be determined.

Compared to radio astronomy there are different practical considerations in (u,v)-plane coverage for an X-ray synthesis telescope. Because the earth's rotation causes the projected baseline $\vec{b}(t)$ of an

interferometer to change continually, successive radio observations correspond to different locations in the (u,v)-plane. Although not always desirable, this effect is extensively used to extend (u,v)-plane coverage using the techniques of earth-rotation synthesis. For a synthesis telescope in an earth-orbiting satellite the X-ray astronomer has greater control. By rotating the telescope to compensate for orbital motion, he can freeze his position in the (u,v)-plane; not compensating ("orbital synthesis") gives the same benefits as earth rotation synthesis. Deliberate rotation of the telescope can provide the maximum possible extension of (u,v)-plane coverage, on a wide range of time scales under observer control.

A second difference is that, while a radio interferometer with N dishes or elements can have up to N(N-1)/2 baselines, the choice of those baselines is clearly not independent. Except as discussed in section (c) below, the parameters chosen for one subcollimator of an X-ray synthesis telescope do not affect the parameters for the other subcollimators, thereby providing the X-ray astronomer with more flexibility in the choice of "baselines".

(b) Finite Bins.

A modest practical limitation comes from the necessity of binning the data into finite angular bins. The position resolution of the counter and telemetry considerations will determine how many independent bins can be used for each subcollimator. For M bins, the coarseness of the spatial binning will reduce the measured visibility by a factor

$$\eta_M \equiv V_M/V_\infty \qquad (11)$$

where V_M is the measured visibility for M bins and $V_\infty = \lim_{M\to\infty} V_M$. From equation 6,

$$V_M = \frac{2}{p} \sum_{k=1}^{M} e^{i\frac{2\pi}{p}\theta_k} N_k \qquad (12)$$

where

$$N_k = \int_{\theta_k - \frac{p}{2M}}^{\theta_k + \frac{p}{2M}} N(\theta)\, d\theta \qquad (13)$$

and

$$\theta_k = -\frac{P}{2} + \frac{(2k-1)}{2}\frac{P}{M} \qquad k = 1, 2, \ldots M$$

For $N(\theta)$ of the expected form, $N(\theta) = a + b\cos(\frac{2\pi\theta}{p} + \theta_0)$ it can be shown that $\eta_M = \frac{M}{\pi}\sin(\frac{\pi}{M})$; this dependence is shown in figure 5.

(c) Aperture Orientation.

In the important practical case where detector position sensitivity is primarily one-dimensional and in the same direction for all sub-collimators, it is important to know how this constrains the choice of grid aperture orientations. Let β be the angle between the direction of best detector resolution and the collimator resolution. The case of $\beta = 0°$ was implicitly assumed in the discussion on Section 3. If w is the collimator width or detector resolution in the other dimension, (whichever is smaller), then the effect of $\beta \neq 0°$ is equivalent to degrading the detector resolution by (w tan β). If L is the collimator

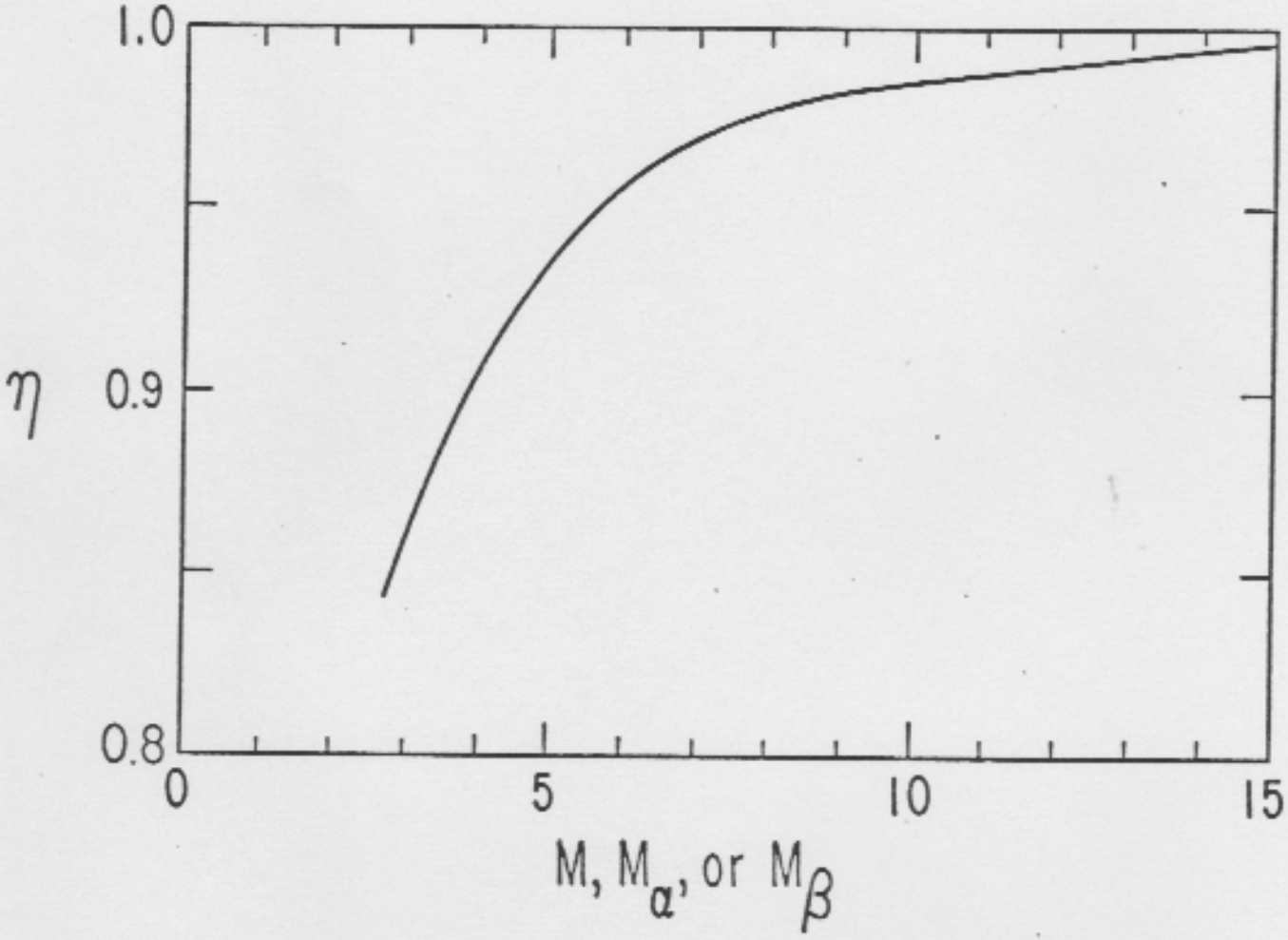

Figure 5. Variation of η with M, M_α, or M_β

length over which response pattern repeats, then it is easy to show that the signal-to-noise ratio is reduced over the $\beta = 0°$ case by a factor

$$\eta_\beta = \frac{M_\beta \sin (\pi/M_\beta}{\pi} \qquad (14)$$

where $M_\beta = L/w \tan \beta$

Thus for subcollimators with a length/width ratio of 10, orientations with $|\beta|$ up to 80° are quite feasible as shown in Figure 5.

(d) Relative Visibility and Higher Harmonics

Since the transmission pattern $\Lambda(\theta)$ contains many harmonics, in principle each subcollimator could yield a set of visibility functions

$$V_n = \frac{2AF\ \Delta t}{n^2\ \pi^2}\ e^{i\frac{2\pi n}{P} x_n} \qquad n = 1, 3, 5 \ldots \qquad (15)$$

and thereby reduce the number of subcollimators required in a Fourier-transform telescope. In practice, however, the visibility from even the next harmonic (n=3) is reduced by a factor of 9 and requires a factor of 3 improvement in detector spatial resolution. In addition, any imperfections or misalignments reduce the visibility of the higher harmonics disproportionately. Thus except for relatively low-resolution subcollimators, with the best signal-to-noise ratio and the least susceptibility to imperfections and misalignments, the information content of the higher harmonics will be small.

Ignoring the higher harmonics, we can fully characterize the output of a subcollimator by N, the total number of detected counts, and v, the relative visibility:

$$v \equiv \frac{1}{0.81\ \eta_M}\ \frac{V}{s} \tag{16}$$

where s is the average count rate, N/M, in each of the M bins. From this definition an unresolved source and zero background correspond to $|v| = 1$, while either a resolved source or a finite background counting rate will give $|v| < 1$.

(e) Signal-to-Noise Ratio

We can obtain a simple relationship between the signal-to-noise ratio and the parameters (v,N) that describe a given subcollimator measurement. For M bins, the distribution $N(\theta)$ can be approximated by

$$N_k = \frac{N}{M}\left(1 + v_M \cos\frac{2\pi}{P}(\theta_k - \phi)\right) \tag{17}$$

$$k = 1,\ldots,M.$$

The visibility function

$$V_M = 2\sum_{k=1}^{M} N_k\, e^{i\frac{2\pi}{P}\theta_\phi} \tag{18}$$

with amplitude

$$|V_M| = N|v_M|. \tag{19}$$

The variance of V_M may be calculated from

$$\text{var } V_M = 2^2\sum_{k=1}^{M} N_k\, e^{i\frac{4\pi}{P}\theta k} \tag{20}$$

$$= 2N$$

and the signal-to-noise ratio of V_M then becomes

$$R = \frac{V_M}{\sigma_{V_M}} = \frac{Nv_M}{\sqrt{2N}} = \sqrt{\frac{N}{2}}|v_M| \qquad (21)$$

(f) Misalignment Error.

The effect of misalignment by translation of the two grids perpendicular to the optical axis to first order merely moves the transmission "fringes" without changing their shapes. Its effects can be removed by in-flight monitoring of the grid locations. Rotation, on the other hand, distorts the fringes. It does this, not by reducing the net transmission, but by tending to flatten the peaks of the triangle function $\Lambda(\theta)$. We now describe the effect of rotational misalignment in a quantitative manner.

A misalignment consisting of a rotation through a small angle α, for a subcollimator with width w, grid separation L, and aperture δ, spreads the angular response maximum by $\Delta\theta$, where

$$\Delta\theta = \frac{\alpha w}{\delta} P \ . \qquad (22)$$

In analogy to equations 11-14, the observed visibility is reduced by a factor $N_\alpha = \frac{M\alpha}{\pi} \sin \frac{\pi}{M\alpha}$ (Figure 5), Where $M_\alpha = P/\Delta\theta = \delta/\alpha w$

As a reference point we can calculate α such that the visibility is reduced to 90% of its peak value. This occurs when $M_\alpha \simeq 5$ or $\alpha = 0.2\ \delta/w$.

As an example, w = 10 cm and δ = 50μ (which would yield P = 1 arc sec for L = 10m) would need rotational stability of ± 20 arc sec.

Note that the tolerance requirements are $\sim \frac{\delta}{w}$, not $\frac{\delta}{L}$ as in the case of multigrid systems. Since the subcollimator width, w, is normally much less than the separation, L, this results in a relative immunity to structural distortions. In a practical situation one could maintain rotational alignment with a servo system, if a rigid structure were not possible to achieve easily.

5. APERTURE EFFICIENCY COMPARISONS AMONG GRID TELESCOPES

As mentioned earlier, one can construct hard X-ray imaging systems with one, two, or many grids. Each approach has specific merits and finds some applications. One-grid systems are simple and have high aperture efficiency (~ 50%), defined as the fraction of total detector area exposed to a point source. High angular resolution is difficult to achieve without large mask-detector separations, however [15]. The two-grid devices discussed here have somewhat lower aperture efficiency but may have high angular resolution. Finally, an n-grid telescope can have good sidelobe rejection, but will have poor aperture efficiency if regarded as an imaging device.

Table 1 summarizes these points for a model one-dimensional imaging system with m pixels. We can define m as the ratio of field-of-view angle to beam width (FWHM); a simple on/off chopping system with a pencil beam would have m=2 and would efficiently deal with known point sources with known background fields. Alternatively, if one cannot confidently predict where a background field may exist, $m \geq 10$ is desirable to eliminate confusion [14]. The one and two-grid schemes multiplex the image, since each detector position-resolution element may receive counts from the entire field of view. Although this may adversely affect the signal-to-noise ratio for weak sources in the presence of strong sources, it provides a large increase in sensitivity for isolated sources when their location is not known a priori.

6. CONCLUSIONS

We have shown that a two-grid modulation collimator for hard X-rays naturally measures the Fourier components of an angular distribution, and is thus exactly analogous to a two-element interferometer for radio astronomy. This permits a full imaging analysis using the highly developed techniques of aperture synthesis. A two-grid collimator has two major simplifications in comparison with other X-ray imaging schemes. Firstly, the position sensitivity of the detector does not need to be high in order to achieve high angular resolution; one can measure each Fourier component with a relatively large subcollimator. Secondly, a two-grid collimator does not present problems of structural rigidity

TABLE 1

Aperture Efficiencies, m Pixels

Telescope Type	Number of Grids	Theoretical Aperture Efficiency (percent)	Multiplex	Applications	Limiting Technical Areas
Multiple Pinhole	1	50	Yes	Low Resolution	Detector Spatial Resolution
Fourier Transform	2	25	Yes	High Resolution	Grids
Pencil Beam	>2	100/m	No	High Contrast	Structure

except for a single motion, namely relative rotation of the two grids. Thus if rotation can be compensated, the telescope structure will be relatively immune to distortions induced, for example, by thermal gradients. Thus the Fourier-transform telescope can combine high aperture efficiency, the multiplex advantage, and structural and detector requirements well suited to present-day technology.

ACKNOWLEDGEMENTS

Part of this work was done in conjunction with the NASA Hard X-ray Imaging Facility Definition Team whose membership consisted of R.L. Blake, C.J. Crannell, G. Garmire, H.S. Hudson, R.P. Lin, L.E. Peterson, Z. Svestka and H.F. van Beek.

This work was supported by the National Science Foundation under grant ATM-7906345 and by NASA 5-22375.

REFERENCES

1. Oda, M., 1965, Appl.Opt., 4, 143.
2. Bradt, H., Garmire, G., Oda, M., Spada, G., Sreekantan, B., and Gorenstein, P., 1968, Space Sci.Rev., 8, 471.
3. Schnopper, H.W., Thompson, R.J., Watt, S., 1968, Space Sci.Rev., 8, 534.
4. van Beek, H.F., 1975, Space Sci. Instrumentation, 2, 197.
5. Mertz, L., 1965, Tranformations in Optics, Wiley.
6. Ables, J.G., 1968, Proc.Ast.Soc. Australia, 1, 172.
7. Dicke, R.H., 1968, Ap.J. (Letters), 153, L101.
8. Gunson, J., and Polychronopulos, B., 1976, Mon.Not.R.Ast.Soc., 177, 485.
9. Fenimore, E., 1978, Appl.Opt., 17, 3562.
10. Makishima, K., Miyamoto, S., Murakami, T., Nishimura, J., Oda, M., Ogawara, Y., and Tawara, Y., in van der Hucht, K., and Vaiana, G.S. (eds.) New Instrumentation in Space Astronomy (New York: Pergamon).
11. Fomalont, E.B., and Wright, M.C.H., 1974, in G.L. Verschuur and K.I. Kellermann (eds.) Galactic and Extragalactic Radio Astronomy (New York: Springer), p. 256.
12. Bracewell, R. and Riddle, A.T., 1968, Ap.J., 150, 427.
13. Christiansen, W.N., and Hogbom, J.A., 1969, Radiotelescopes (Cambridge)
14. Kraus, J.D., 1966, Radio Astronomy (New York: McGraw Hill).
15. Hudson, H.S. and Lin, R.P., 1978, Space Sci.Inst., 4, 101.